Finite element analysis of CFT columns subjected to pure bending moment

H.-T. Hu[*1], F.-C. Su[1] and M. Elchalakani[2]

[1]*Department of Civil Engineering and Sustainable Environment Research Center*
National Cheng Kung University, Tainan, Taiwan 701, R.O.C.
[2]*School of Architectural, Civil and Mechanical Engineering, Victoria University*
Footscray Park Campus, Ballarat Road, Vic 8001, Australia

Abstract. Proper material constitutive models for concrete-filled tube (CFT) columns of circular cross section and subjected to pure bending moment are proposed. These material models are implemented into the Abaqus finite element program and verified against experimental data. It has been shown that the steel tube does not provide good confining effect to the concrete core when the CFT columns is subjected to pure bending moment. When the diameter-to-thickness ratio of the CFT columns is small, the behavior of the CFT column is the same as the steel tube without a concrete core.

Keywords: concrete-filled tube; lateral confining pressure; finite element analysis.

1. Introduction

A concrete-filled tube (CFT) column consists of a steel tube filled with concrete. The concrete core adds stiffness and compressive strength to the tubular column and reduces the potential of inward local buckling. On the other hand, the steel tube acts as a longitudinal and a lateral reinforcement for the concrete core to resist tension, bending moment, and shear and to prevent the concrete from spalling. Due to the benefit of composite action of both materials, the CFT columns provide excellent seismic resistant structural properties such as high strength, high ductility and large energy absorption capacity. In addition, the steel tube acts as both erection steel and forming for the composite column during construction. Thus, a considerable amount of labor, materials and construction costs can be reduced. As a result, CFT columns have gained popularity in supporting heavy loads in high-rise buildings, bridges and offshore structures. Various experimental and analytical studies have been performed on CFT columns (Furlong 1963, Knowles and Park 1969, Ge and Usami 1992, Boyd *et al.* 1995, Bradford 1996, Shams and Saadeghvaziri 1997, Schneider 1998, Roeder *et al.* 1999, Zhang and Shahrooz 1999, Uy 2000, Elchalakani *et al.* 2001, Elremaily and Azizinamini 2002, Hu *et al.* 2003, Hu *et al.* 2005, Lu *et al.* 2007).

It is known that the ultimate strengths of CFT columns are influenced by their constituent material properties such as the compressive strength of the concrete, the yield strength of the steel, and the nonlinear behavior of these two materials. In addition, the ultimate strengths of CFT columns are also

---

influenced by the concrete confining pressure and the geometric properties of the tubes such as the shape of the cross section and the diameter-to-thickness ratio.

It is well known that the CFT columns with circular cross section provide better confining pressure than those with rectangular cross section. Therefore, the aim of this investigation is to employ the nonlinear finite element program Abaqus (2009) to perform numerical simulations of CFT columns with circular cross section and subjected to pure bending moment. To achieve this goal, proper material constitutive models for steel tube and concrete core are proposed. Then the proposed material constitutive models are verified against experimental data of Elchalakani *et al.* (2001). Finally, the influence of the concrete confining pressure and the diameter-to-thickness ratio of the columns on the behavior of CFT columns are studied and discussed.

2. Material properties and constitutive models

The cross section of the CFT columns in this investigation is circular as shown in Fig. 1. Constitutive models of these materials are proposed and discussed as follows.

2.1 Steel tube

In the analysis, the Poisson's ratio v_S and the elastic modulus E_S of the steel tube are assumed to be 0.3 and 204 GPa, respectively. The uniaxial behavior of the steel tube is modeled by a bilinear model (Fig. 2), where f_y and f_u are the yield stress and the ultimate stress of the steel tube, respectively. When the steel tube is subjected to multiple stresses, a von Mises yield criterion is employed to define the initial yield surface, which is written as

$$F = \sqrt{3J_2} - f_y = \frac{1}{\sqrt{2}}\sqrt{(\sigma_1 - \sigma_2)^2 + (\sigma_2 - \sigma_3)^2 + (\sigma_3 - \sigma_1)^2} - f_y = 0 \qquad (1)$$

where J_2 is the second stress invariant of the stress deviator tensor and σ_1, σ_2, and σ_3 are the principal stresses. Figure 3 shows the von Mises yield surface in the three-dimensional principal stress space. The response of the steel tube is modeled by an elastic-hardening plastic theory with isotropic hardening rule and associated flow rule. When plastic deformation occurs, there should be a certain
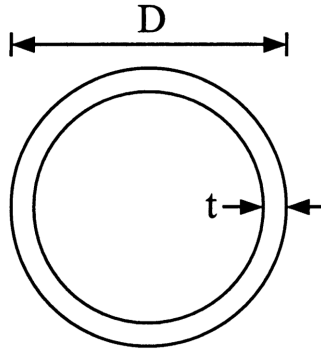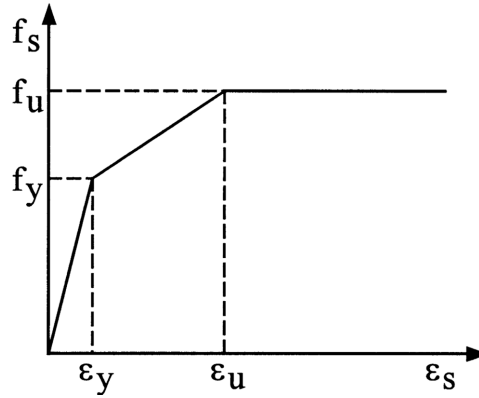

Fig. 1 Cross section of CFT
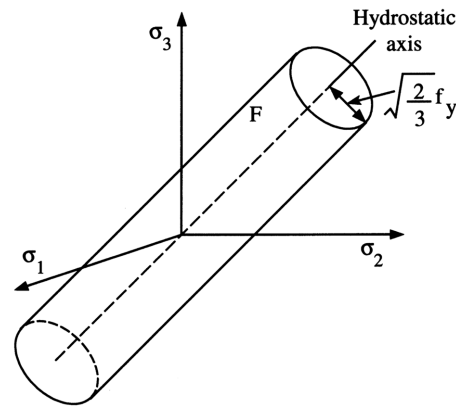
Fig. 2 Bilinear stress-strain curve of steel

Fig. 3 von Mises yield surface in the three-dimensional principal stress space

parameter to guide the expansion of the yield surface. A commonly used approach is to relate the multidimensional stress and strain conditions to a pair of quantities, namely, the effective stress f_S and effective strain ε_S, such that results obtained following different loading paths can all be correlated by means of the equivalent uniaxial stress-strain curve. In this investigation, the uniaxial stress-strain relationship given in Fig. 2 is used as the equivalent uniaxial stress-strain curve for steel. As the result, the subsequent yield surface of steel can be written as

$$F = \sqrt{3J_2} - f_S = \frac{1}{\sqrt{2}}\sqrt{(\sigma_1 - \sigma_2)^2 + (\sigma_2 - \sigma_3)^2 + (\sigma_3 - \sigma_1)^2} - f_S = 0 \qquad (2)$$

2.2 Concrete

The Poisson's ratio v_c of concrete under uniaxial compressive stress ranges from 0.15 to 0.22, with a representative value of 0.19 or 0.20 (ASCE 1982). In this study, the Poisson's ratio of concrete is assumed to be 0.2.
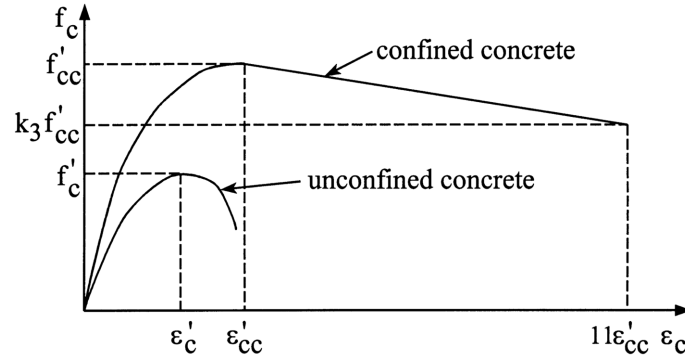
Fig. 4 Equivalent uniaxial stress-strain curve for concrete

Let the uniaxial compressive strength and the corresponding strain of the unconfined concrete be f_c' and ε_c' (Fig. 4). The value of ε_c' is usually around the range of 0.002 to 0.003. A representative value 0.002 is used in the analysis. When concrete is subjected to laterally confining pressure, the uniaxial compressive strength f_{cc}' and the corresponding strain ε_{cc}' (Fig. 4) are much higher than those of unconfined concrete. The relations between f_{cc}', f_c' and between ε_{cc}', ε_c' are estimated by the following equations (Mander *et al.* 1988)

$$f_{cc}' = k_4 f_c' + k_1 f_l \tag{3}$$

$$\varepsilon_{cc}' = \varepsilon_c' \left(1 + k_2 \frac{f_l}{f_c'}\right) \tag{4}$$

where f_l represents the confining pressure around the concrete core. k_1 and k_2 are constants and can be obtained from experimental data. Meanwhile, the constants k_1 and k_2 are set as 4.1 and 20.5 based on the studies of Richart, Brandtzaeg and Brown (1928). The original form of Eq. (3) was proposed for concrete subjected to hydrostatic pressure (Mander *et al.* 1988) and did not contain the strength factor k_4. For CFT columns subjected to bending moment, part of the concrete may be subject to tensile stress, which is different from the hydrostatic pressure condition. Therefore, a strength factor k_4 is introduced by the authors (Hu *et al.* 2005) with the limitation $k_4 \leq 1$.

Because the concrete in the CFT columns is usually subjected to triaxial compressive stresses, the failure of concrete is dominated by the compressive failure surface expanding with increasing hydrostatic pressure. Hence, a linear Drucker-Prager yield criterion G (Fig. 5) is used to model the yield surface of concrete, which is expressed as

$$G = t - p \tan \beta - d = 0 \tag{5}$$

where

$$p = -(\sigma_1 + \sigma_2 + \sigma_3)/3 \tag{6.a}$$

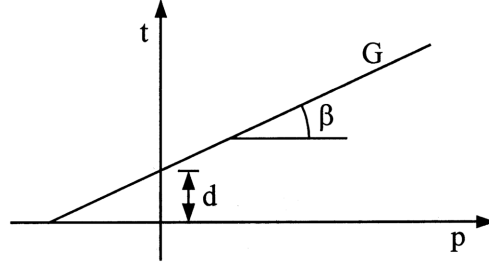$$d = \left(1 - \frac{\tan \beta}{3}\right) f_{cc}' \tag{6.b}$$

Fig. 5 Linear Drucker-Prager yield criterion for concrete

$$t = \frac{\sqrt{3J_2}}{2}\left[1 + \frac{1}{K} - \left(1 - \frac{1}{K}\right)\left(\frac{r}{\sqrt{3J_2}}\right)^3\right] \tag{6.c}$$

$$r = \left[\frac{9}{2}(S_1^3 + S_2^3 + S_3^3)\right]^{1/3} \tag{6.d}$$

and S_1, S_2, and S_3 are principal stress deviators. The constants K and β are material parameters determined from experimental data. In the analysis, K and β are set to 0.8 and 20°, respectively (Hu *et al*. 2005).

The response of the concrete is also modeled by an elastic-hardening plastic theory with isotropic hardening rule and associated flow rule. The stress-strain relationship proposed by Saenz (1964) has been widely adopted as the uniaxial stress-strain curve for concrete and it has the following form

$$f_c = \frac{E_c\varepsilon_c}{1 + (R + R_E - 2)\left(\dfrac{\varepsilon_c}{\varepsilon'_{cc}}\right) - (2R - 1)\left(\dfrac{\varepsilon_c}{\varepsilon'_{cc}}\right)^2 + R\left(\dfrac{\varepsilon_c}{\varepsilon'_{cc}}\right)^3}$$

where

$$R = \frac{R_E(R_\sigma - 1)}{(R_\varepsilon - 1)^2} - \frac{1}{R_\varepsilon}, \qquad R_E = \frac{E_c\varepsilon'_{cc}}{f'_{cc}} \tag{7}$$

and $R_\sigma = 4$, $R_\varepsilon = 4$ may be used (Hu and Schnobrich 1989). The initial modulus of elasticity of concrete E_c is highly correlated to its compressive strength and can be calculated with reasonable accuracy from the empirical equation (ACI 2005)

$$E_c = 4700\sqrt{f'_{cc}}\,\text{MPa} \tag{8}$$

In the analysis, Eq. (7) is taken as the equivalent uniaxial stress-strain curve for concrete when the concrete strain ε_c is less than ε'_{cc} (Fig. 4). When $\varepsilon_c > \varepsilon'_{cc}$, a linear descending line is used to model the softening behavior of concrete. If k_3 is defined as the material degradation parameter, the descending line is assumed to be terminated at the point where $f_c = k_3 f'_{cc}$ and $\varepsilon_c = 11\varepsilon'_{cc}$ (Hu *et al*. 2005).

Generally, the parameters f_l, k_3 and k_4 should be provided in order to completely define the equivalent uniaxial stress-strain relation. These three parameters apparently depend on the cross-sectional geometry and material properties. Consequently, their appropriate values are determined by matching the numerical results with experimental data via parametric studies.

3. Finite element model for CFT columns

The experiment set up for CFT column subjected to pure bending moments carried out by Elchalakani *et al*. (2001) is shown in Fig. 6. The CFT beam is tested in pure bending rig, such rig could apply pure bending over the middle span. Also, prevent the axial or shear forces. When the CFT columns were cast, an end cap (thin steel plate) was used to cast the concrete while the steel tube was in the vertical position. The end cap was removed and the ends of the specimens were left uncapped to allow slippage to occur. This was believed to be the worst case in regards to loss of composite action.

Due to symmetry, only one fourth of the CFT column is analyzed (Fig. 7). Symmetric boundary conditions are enforced on the symmetric planes, which are $u_3 = 0$ on the left surface of the element mesh and $u_1 = 0$ on the front surface of the element mesh surface. To simulate the wheel support, the displacements u_2 for the nodes at the mid-depth of the right edge of the element mesh are all set to zero.

In the finite element mesh, both the concrete core and the steel tube are modeled by 27-node solid elements (three degrees of freedom per node) with reduced integration rule. The interface between concrete core and steel tube is modeled by a pair of contact surfaces. The nodes of concrete core and steel tube are connected through the contact surfaces that require matching meshes of the two bodies. The contact surfaces can model infinitesimal sliding and friction (Abaqus 2009) between concrete core and steel tube. The friction coefficient used in all the analyses is $\mu_S = 0.25$ (Hu *et al*. 2005). Through the
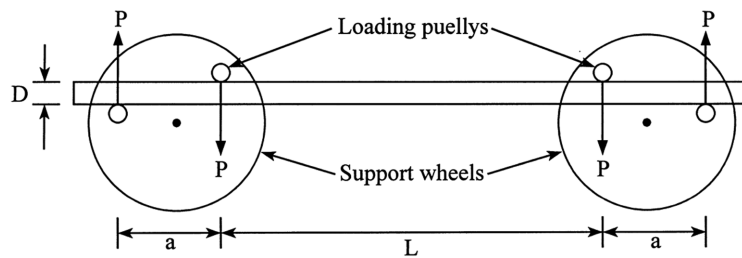

Fig. 6 Experimental set up for CFT column subjected to pure bending moment
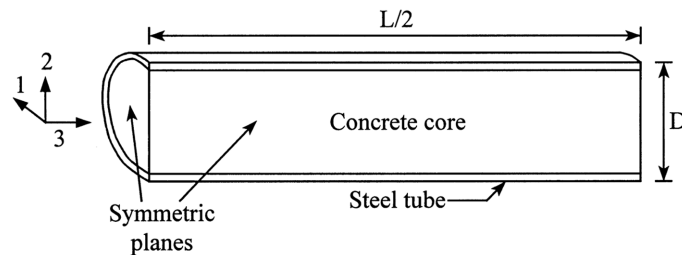

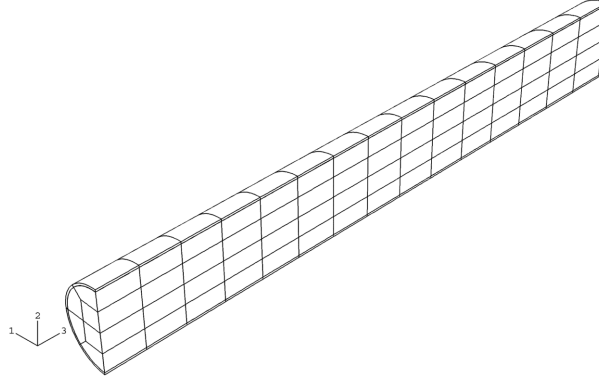Fig. 7 Conceptual sketch and finite element modeling of CFT column

Fig. 8 Finite element mesh for CFT columns

contact surfaces, concrete core and steel tube are allowed to either contact or separate but not to penetrate each other.

Convergent studies of the finite element meshes have been done by the authors using various element sizes for CFT columns (Su 2004). It has been shown that the numerical results are not sensitive to the element sizes and mesh refinements. As a result, the mesh shown in Fig. 8 is used for CFT columns through out the analyses.

4. Numerical analysis

In this section, the experimental data from Elchalakani *et al.* (2001) are used to verify and calibrate the proposed material model for CFT columns. There are twelve specimens in the experiment, which are CBC0-A, CBC0-B, CBC0-C, CBC1, CBC2, CBC3, CBC4, CBC5, CBC6, CBC7, CBC8 and CBC9. The diameter-to-thickness ratio D/t of them varies from 12.8 to 109.9. The dimensions and material properties of these CFT columns are shown in Table 1.

Due to the capacity of the experimental equipments, the tube diameters in this investigation are in the range from 30 mm to 110 mm. Although, these tube diameters are much smaller than those used in engineering applications, it is known that the ultimate strengths of the CFT columns highly depend on the diameter-to-thickness ratio D/t. Therefore, in the Eurocode 4 specification (Office for Official Publications of the European Communities 1994), the diameter-to-thickness ratio is limited to

$$D / t \leq 90 \times 235 / f_y \quad (f_y \text{ in MPa}) \tag{9}$$

In addition, in the AIJ specification (Architectural Institute of Japan 1991), the diameter-to-thickness ratio is limited to

$$D / t \leq 1.5(240 / G) \tag{10a}$$

$$G = \min(f_y, 0.7fu) \quad (f_y \text{ and } f_u \text{ in ton} / \text{cm}^2) \tag{10b}$$

In this investigation, the main focus is on the influence of the diameter-to-thickness ratio D/t to the

Table 1 Geometry and material properties of CFT columns

Specimen	D (mm)	t (mm)	D/t	L (mm)	$f_c'(MPa)$	$f_y(MPa)$
CBC0-C	109.9	1.00	109.9	800	23.4	400
CBC0-B	110.4	1.25	88.3	800	23.4	400
CBC0-A	110.9	1.50	73.9	800	23.4	400
CBC1	101.8	2.53	40.2	800	23.4	365
CBC2	88.64	2.79	31.8	800	23.4	432
CBC3	76.32	2.45	31.2	800	23.4	415
CBC4	89.26	3.35	26.6	800	23.4	412
CBC5	60.65	2.44	24.9	800	23.4	433
CBC6	76.18	3.24	23.5	800	23.4	456
CBC7	60.67	3.01	20.2	800	23.4	408
CBC8	33.66	1.98	17.0	800	23.4	442
CBC9	33.78	2.63	12.8	800	23.4	460

ultimate strengths of the CFT columns and not on the physical scales of the tube diameter D or the tube thickness t.

4.1 Simulation of ultimate stress f_u and ultimate strain ε_u of steel

According to the material tested data Elchalakani *et al.* (2001), the ultimate strain ε_u of the steel tube varies between 0.0022 and 0.0030 with a mean value 0.0026. Therefore, the mean value of the ultimate strain $\varepsilon_u = 0.0026$ is used in the numerical analyses. Since the ultimate stress f_u of steel tube for CFT is rather diverse in the experimental tests, various ultimate stresses of the steel tubes, *i.e.*, $f_u = 1.7f_y$, $1.8f_y$, $1.9f_y$, are simulated for CFT specimens. The moment versus curvature relation of the numerical results and the experimental data for specimen CBC1 are shown in Fig. 9. It can be seen that the result of the curve with $f_u = 1.8f_y$ is closest to the experimental data and the numerical results are not significantly influenced by the ultimate stress of the steel tube. In addition, the value $f_u = 1.8f_y$ has been shown by other investigators to be a fairly good typical value (Wang and Salmon 2006). As the result, $f_u = 1.8f_y$ is adopted for the rest part of the numerical analyses.
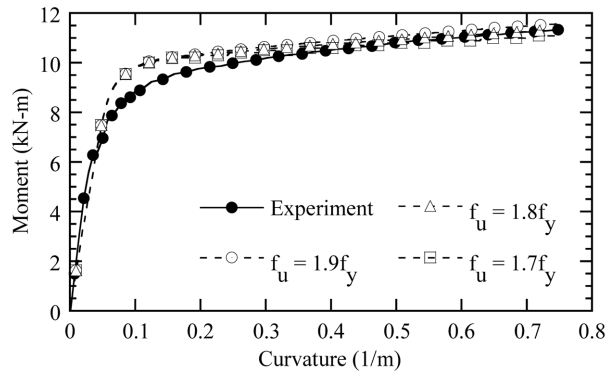

Fig. 9 Simulation of f_u for specimen CBC1 ($f_l = 0$, $k_3 = 0.9$, $k_4 = 0.4$)

4.2 Simulation of the material degradation parameter k_3

The material degradation parameter k_3 varies between 0 and 1. It has been suggested that k_3 is close to 1 for CFT subjected to pure bending (Hu *et al.* 2005). To make a proper selection of k_3, different values of k_3 are simulated for CFT specimen. Those selected k_3 values are $k_3 = 0.6$, 0.8, 0.9 and 1, respectively. The moment versus curvature relation of the numerical results and the experimental data for specimen CBC1 are shown in Fig. 10. It can be seen that the result of the curve with $k_3 = 0.9$ is closest to the experimental data. Similar results are also observed for other specimens. Hence, $k_3 = 0.9$ is adopted for the rest part of the numerical analyses.

4.3 Simulations of f_l and k_4

In this section, all the twelve specimens are analyzed and the results of numerical simulations for these CFT columns are given in Table 2. The curves of moment versus curvature at the midspan of the
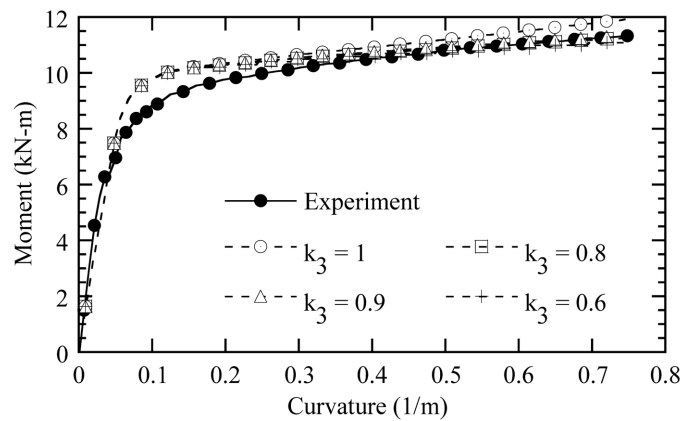
Fig. 10 Simulation of k_3 for specimen CBC1 ($f_l = 0$, $k_4 = 0.4$)

Table 2 Results of numerical simulations

Specimen	D/t	Ultimate Moment (kN-m)		Error (%)	f_l	k_4
		Experiment	Analysis			
CBC0-C	109.9	7.64	7.62	0.26	0	0.6
CBC0-B	88.3	9.08	9.05	0.33	0	0.75
CBC0-A	73.9	11.72	11.80	0.68	0	1.0
CBC1	40.2	11.33	11.34	0.09	0	0.4
CBC2	31.8	10.94	10.97	0.27	0	0.2
CBC3	31.2	6.84	6.83	0.14	0	0.3
CBC4	26.6	11.25	11.23	0.17	0	0.1
CBC5	24.9	3.97	4.12	3.78	0	0.05
CBC6	23.5	9.87	9.63	2.43	0	0.4
CBC7	20.2	5.00	4.90	2.00	0	0.2
CBC8	17.0	0.93	0.94	1.08	0	0.01
CBC9	12.8	1.20	1.25	4.17	0	0.01

CFT columns are plotted against the experiment data in Fig. 11. Generally, the numerical results show good agreement with the experimental data. The moment-curvature curves of these CFT columns exhibit a very ductile behavior before the failure of the specimens occur.

From the results of numerical simulations, we can observe that the lateral confining pressure f_l on the concrete core is zero for all the specimens. This means that CFT subjected to pure bending moment does not have any confining effect at all. This is because a large portion of the concrete cross section is in tension denominated condition and the entire concrete core does not expand in the radial direction too much. As the result, the steel tube can not provide any lateral confining pressure to the concrete core. Though, this phenomenon has been observed by Hu *et al*. (2005) in the analysis of CFT columns subjected to combined axial compressive force and bending moment. However, through the intensive
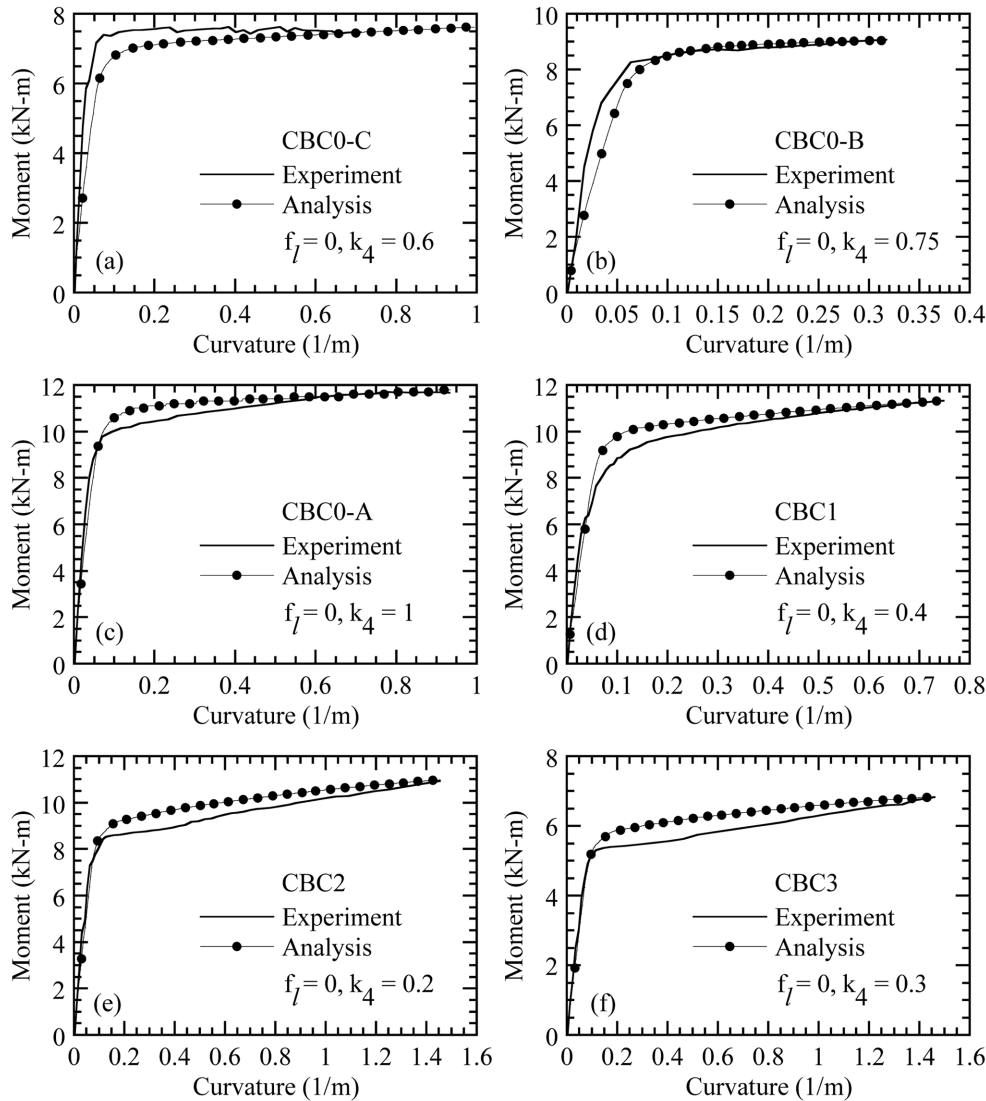

Fig. 11 Moment - curvature relations of CFT columns subjected to pure bending (Continued)
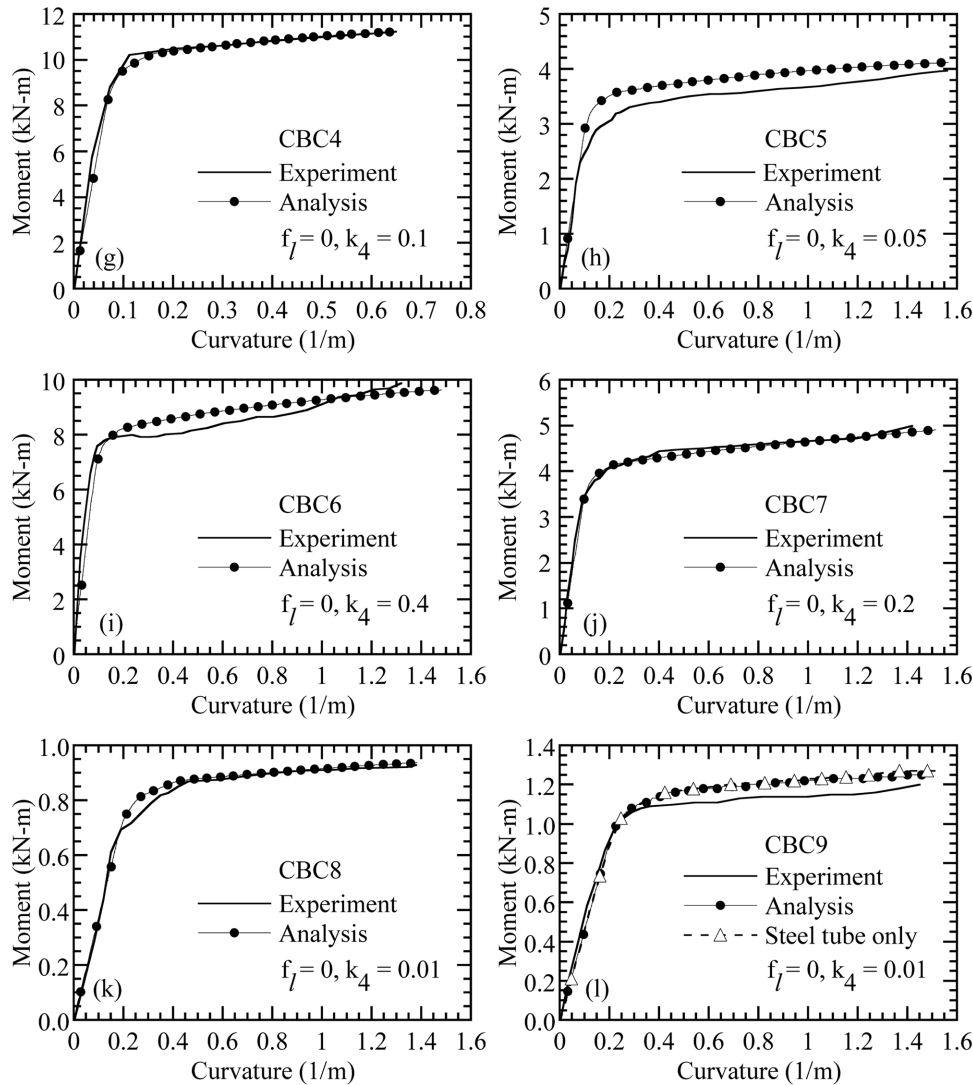
Fig. 11 Continued.

studies of CFT columns subjected to pure bending moments, this phenomenon is fully confirmed. Therefore, it is not suggested to design a CFT column to resist pure bending moment in practice.

The value of the strength factor k_4 versus the diameter-to-thickness ratio D/t is shown in Fig. 12. It can be observed that the D/t ratio has significant influence on the strength factor k_4. When the D/t ratio is great than 74, k_4 seems to decrease with the increase of D/t ratio. However, when the D/t ratio is less than 74, k_4 seems to decrease with the decrease of D/t ratio. When the D/t ratio is small (say D / t < 20), the strength factor k_4 is almost equal to zero, which means the concrete core does not have any capability to resist bending moment. This phenomenon has been further investigated for the CBC9 specimen. In Fig. 11(l), a separate analysis is performed for the steel tube (without concrete core) subjected to pure bending moment. The curve obtained for the steel tube is almost the same as that of the CBC9 CFT column. This confirms that the concrete core is incapable to resist bending moments
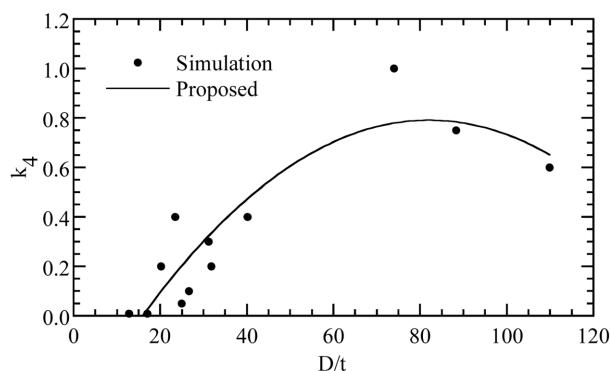
Fig. 12 k_4 versus D/t for CFT columns

when the D/t ratio of a CFT column is small, which is also in a good agreement with the experimental work (Elchalakani *et al.* 2001).

Based on the results of numerical simulations, a curve-fitting equation for k_4 in second order polynomial may be proposed as follows

$$k_4 = -0.4237 + 0.02963(D/t) - 0.0001805(D/t)^2 \tag{11}$$

Fig. 13 shows the typical deformation shapes of CBC1 specimen around the ultimate loading stage. It can be seen that the concrete core and steel tube still keep in contact to each other and no local buckling of the tube takes place. This phenomenon is also observed for other CFT specimens (Su 2004).

5. Conclusions

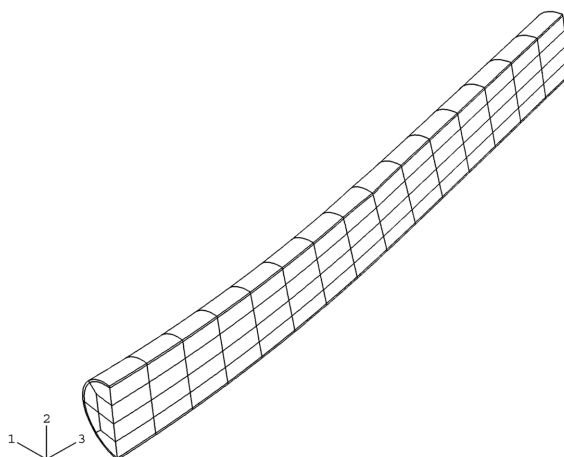In this paper, nonlinear finite element analyses of CFT columns with circular cross section and

Fig. 13 Deformation shape of specimen CBC1

subjected to pure bending moment are performed. Based on the numerical results, the following conclusions may be drawn

(1) In the general sense, the steel tube in the CFT column reinforces the strength of concrete. The main reason is due to the lateral confining pressure f_l. For the CFT column subjected to pure bending moment, the lateral confining pressure does not exist.

(2) When D / t > 74, the strength factor k_4 seems to decrease with the increase of D/t ratio. However, when D / t < 74, k_4 seems to decrease with the decrease of D/t ratio. In addition, when the D/t ratio is small (say D / t < 20), the concrete core does not have any capability to resist the bending moment. As the result, the behavior of CFT column is the same as the steel tube without a concrete core.

Acknowledgments

References

Abaqus, Inc (2009), *Abaqus analysis user's manuals and example problems manuals*, Version 6.9, Providence, Rhode Island.

ACI Committee 318 (2005), *Building code requirements for structural concrete and commentary (ACI 318-05)*, American Concrete Institute, Detroit, Michigan.

Architectural Institute of Japan (1991), *AIJ standards for structural calculation of steel reinforced concrete structures*, Tokyo.

ASCE Task Committee on Concrete and Masonry Structure (1982), *State of the art report on finite element analysis of reinforced concrete*, ASCE, New York.

Bradford, M.A. (1996), "Design strength of slender concrete-filled rectangular steel tubes", *ACI Struct. J.*, **93**(2), 229-235.

Boyd, F.P., Cofer, W.F. and McLean, D. (1995), "Seismic performance of steel-encased concrete column under flexural loading", *ACI Struct. J.*, **92**(3), 355-365.

Elchalakani, M., Zhao, X.L. and Grzebieta, R.H. (2001), "Concrete-filled circular steel tube subjected to pure bending", *J. Constr. Steel. Res.*, **57**(11), 1141-1168.

Elremaily, A. and Azizinamini, A. (2002), "Behavior and strength of circular concrete-filled tube columns", *J. Constr. Steel. Res.*, **58**(12), 1567-1591.

Furlong, R.W. (1963), "Strength of steel-encased concrete beam-columns", *J. Struct. Div-ASCE*, **93**(5), 113-124.

Ge, H.B. and Usami, T. (1992), "Strength of concrete-filled thin-walled steel box columns: experiment", *J. Struct. Eng-ASCE*, **118**(1), 3036-3054.

Hu, H.T., Huang, C.S. and Chen, Z.L. (2005), "Finite element analysis of CFT columns subjected to combined axial force and bending moment", *J. Constr. Steel. Res.*, **61**(12), 1692-1712.

Hu, H.T., Huang, C.S., Wu, M.H. and Wu, Y.M. (2003), "Nonlinear analysis of axially loaded CFT columns with confinement effect", *J. Struct. Eng-ASCE*, **129**(10), 1322-1329.

Hu, H.T. and Schnobrich, W.C. (1989), "Constitutive modelling of concrete by using nonassociated plasticity", *J. Mater. Civil. Eng-ASCE*, **1**(4), 199-216.

Lu, F.W., Li, S.P. and Sun, G. (2007), "A study on the behavior of eccentrically compressed square concrete-filled steel tube columns", *J. Constr. Steel. Res.*, **63**(7), 941-948.

Knowles, R.B. and Park, R. (1969), "Strength of concrete filled steel tubular columns", *J. Struct. Div-ASCE*, **95**(12), 2565-2587.

Mander, J.B., Priestley, M.J.N. and Park, R. (1988), "Theoretical stress-strain model for confined concrete", *J.*

Struct. Eng-ASCE, **114**(8), 1804-1823.

Office for Official Publications of the European Communities (1994), EN 1994 - Eurocode 4 - Design of composite steel and concrete structures, Luxembourg.

Richart, F.E., Brandtzaeg, A. and Brown, R.L. (1928), *A study of the failure of concrete under combined compressive stresses*, Bulletin 185, University of Illinois Engineering Experimental Station, Champaign, Illinois.

Roeder, C.W., Cameron, B. and Brown, C.B. (1999), "Composite action in concrete filled tubes", *J. Struct. Eng*-ASCE, **125**(5), 477-484.

Saenz, L.P. (1964), Discussion of "Equation for the stress-strain curve of concrete" by Desayi, P. and Krishnan, S., *ACI J.*, **61**, 1229-1235.

Schneider, S.P. (1998), "Axial loaded concrete-filled steel tubes", *J. Struct. Eng*-ASCE, **124**(10), 1125-1138.

Shams, M. and Saadeghvaziri, M.A. (1997), "State of the art of concrete-filled steel tubular columns", *ACI Struct. J.*, **94**(5), 558-571.

Schneider, S.P. (1998), "Axial loaded concrete-filled steel tubes", *J. Struct. Eng*-ASCE, **124**(10), 1125-1138.

Su, F.C. (2004), *Numerical analysis of concrete filled tubes subjected to pure bending*, M.S. thesis (in chinese), Department of Civil Engineering, National Cheng Kung University, Tainan, Taiwan, R.O.C.

Uy, B. (2000), "Strength of concrete filled steel box columns incorporating local buckling", *J. Struct. Eng*-ASCE, **126**(3), 341-352.

Wang, C.K. and Salmon, C.G. (2006), *Reinforced Concrete Design*, 7th Edition, John Wiley and Sons.

Zhang,W. and Shahrooz, B.M. (1999), "Comparison between ACI and AISC for concrete-filled tubular columns", *J. Struct. Eng*-ASCE, **125**(11), 1213-1223.

CC